

AD-A035 850

NAVAL POSTGRADUATE SCHOOL MONTEREY CALIF
PREDICTION OF THE FAR-FIELD BEAM PATTERN OF A RANDOM NOISE SOUR--ETC(U)
DEC 76 J T SANCHEZ

F/G 20/1

UNCLASSIFIED

NL

1 OF 1
AD-A
035 850



END
DATE
FILMED
3-24-77
NTIS

U.S. DEPARTMENT OF COMMERCE
National Technical Information Service

AD-A035 850

PREDICTION OF THE FAR-FIELD BEAM PATTERN OF
A RANDOM NOISE SOURCE FROM MEASUREMENTS
MADE IN THE NEAR-FIELD

NAVAL POSTGRADUATE SCHOOL
MONTEREY, CALIFORNIA

DECEMBER 1976

ADA 035850

NAVAL POSTGRADUATE SCHOOL

Monterey, California



THESIS

PREDICTION OF THE FAR-FIELD BEAM PATTERN
OF A RANDOM NOISE SOURCE FROM
MEASUREMENTS MADE IN THE NEAR-FIELD

by

Jorge Trelles Sánchez

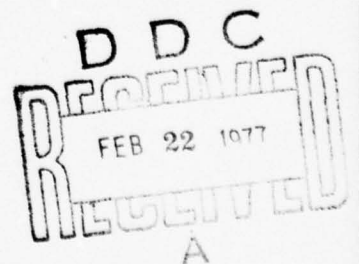
December 1976

Thesis Advisor:

G. L. Sackman

Approved for public release; distribution unlimited.

REPRODUCED BY
NATIONAL TECHNICAL
INFORMATION SERVICE
U. S. DEPARTMENT OF COMMERCE
SPRINGFIELD, VA. 22161



UNCLASSIFIED

SECURITY CLASSIFICATION OF THIS PAGE (When Data Entered)

REPORT DOCUMENTATION PAGE		READ INSTRUCTIONS BEFORE COMPLETING FORM
1. REPORT NUMBER	2. GOVT ACCESSION NO.	3. RECIPIENT'S CATALOG NUMBER
4. TITLE (and Subtitle) Prediction of the Far-Field Beam Pattern of a Random Noise Source from Measurements Made in the Near-Field		5. TYPE OF REPORT & PERIOD COVERED Master's Thesis; December 1976
7. AUTHOR(s) Jorge Trelles Sánchez		6. PERFORMING ORG. REPORT NUMBER
9. PERFORMING ORGANIZATION NAME AND ADDRESS Naval Postgraduate School Monterey, California 93940		8. CONTRACT OR GRANT NUMBER(s)
11. CONTROLLING OFFICE NAME AND ADDRESS Naval Postgraduate School Monterey, California 93940		10. PROGRAM ELEMENT, PROJECT, TASK AREA & WORK UNIT NUMBERS
14. MONITORING AGENCY NAME & ADDRESS (if different from Controlling Office) Naval Postgraduate School Monterey, California 93940		12. REPORT DATE December 1976
		13. NUMBER OF PAGES 53
		15. SECURITY CLASS. (of this report) Unclassified
		15a. DECLASSIFICATION/DOWNGRADING SCHEDULE
16. DISTRIBUTION STATEMENT (of this Report) Approved for public release; distribution unlimited.		
17. DISTRIBUTION STATEMENT (of the abstract entered in Block 20, if different from Report)		
18. SUPPLEMENTARY NOTES		
19. KEY WORDS (Continue on reverse side if necessary and identify by block number) Far-Field Beam Pattern Beam Pattern Prediction		
20. ABSTRACT (Continue on reverse side if necessary and identify by block number) A theory is presented for computing the far field beam patterns from distributed random noise sources. The theoretical model utilizes the Green's Function for the wave equation and the space-time autocorrelation function for determining the radiation from a randomly vibrating area. The actual far field beam pattern of a horn speaker in an anechoic chamber was obtained, and also near field measurements were		

DD FORM 1473
1 JAN 73
(Page 1)

EDITION OF 1 NOV 68 IS OBSOLETE
S/N 0102-014-6601

UNCLASSIFIED
SECURITY CLASSIFICATION OF THIS PAGE (When Data Entered)

UNCLASSIFIED

SECURITY CLASSIFICATION OF THIS PAGE/When Data Entered:

taken to obtain the correlation distance and the mean square of the particle velocity using the autocorrelation function. Finally a computer program was written to evaluate the integral wave equation by numerical methods. It was found that the critical parameters in the mathematical model were the correlation distance and the frequency limits of integration. Small variations in the correlation distance modified greatly the width of the predicted beam pattern, while changes in the limits of integration had a moderate effect. The Frequency Spectrum was obtained in the anechoic chamber and it was used to determine the limits of integration of the integral solution for the intensity field.

The predicted beam patterns were in satisfactory agreement with the measured far field beam patterns. The differences between them are probably due to inaccuracies in determining the limits of integration and the correlation distance.

ACCESSION NO.	
NTIS	DATE [unclear] <input checked="" type="checkbox"/>
DDC	DATE [unclear] <input type="checkbox"/>
UNCLASSIFIED	<input type="checkbox"/>
JUSTIFICATION	
BY	
CONTRIBUTOR/ACQUISITION UNIT	
S/N	
A	

DD Form 1473
1 Jan 73
S/N 0102-014-6601

UNCLASSIFIED

SECURITY CLASSIFICATION OF THIS PAGE/When Data Entered:

Prediction of the Far-Field Beam Pattern
of a Random Noise Source from
Measurements Made in the Near-Field

by

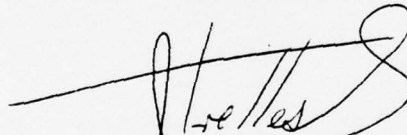
Jorge Trelles Sánchez
Lieutenant, Peruvian Navy

Submitted in partial fulfillment of the
requirements for the degree of

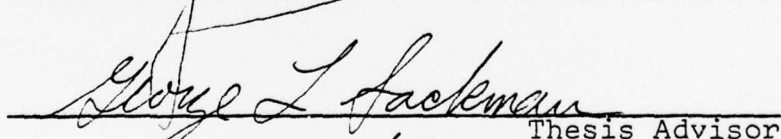
MASTER OF SCIENCE IN ENGINEERING ACOUSTICS

from the
NAVAL POSTGRADUATE SCHOOL
December 1976

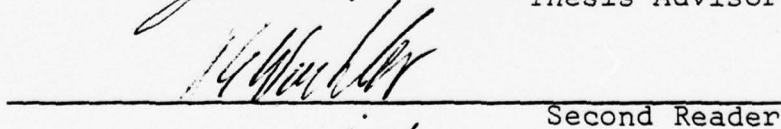
Author



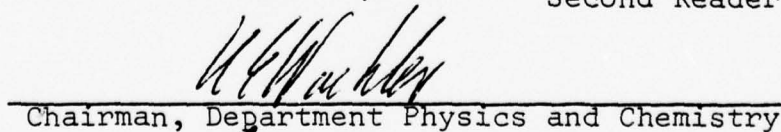
Approved by:



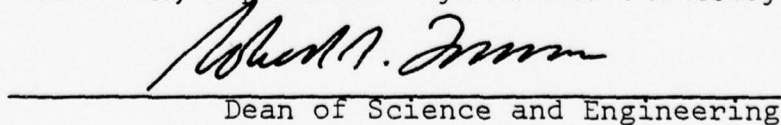
Thesis Advisor



Second Reader



Chairman, Department Physics and Chemistry



Dean of Science and Engineering

ABSTRACT

A theory is presented for computing the far field beam patterns from distributed random noise sources. The theoretical model utilizes the Green's Function for the wave equation and the space-time autocorrelation function for determining the radiation from a randomly vibrating area. The actual far field beam pattern of a horn speaker in an anechoic chamber was obtained, and also near field measurements were taken to obtain the correlation distance and the mean square of the particle velocity using the autocorrelation function. Finally a computer program was written to evaluate the integral wave equation by numerical methods. It was found that the critical parameters in the mathematical model were the correlation distance and the frequency limits of integration. Small variations in the correlation distance modified greatly the width of the predicted beam pattern, while changes in the limits of integration had a moderate effect. The Frequency Spectrum was obtained in the anechoic chamber and it was used to determine the limits of integration of the integral solution for the intensity field.

The predicted beam patterns were in satisfactory agreement with the measured far field beam patterns. The differences between them are probably due to inaccuracies in determining the limits of integration and the correlation distance.

TABLE OF CONTENTS

I. INTRODUCTION - - - - - 7

II. GENERAL THEORY - - - - - 10

III. EXPERIMENTAL RESULT USING A PLANE MODEL - - - - 28

 A. FAR-FIELD MEASUREMENT - - - - - 28

 B. NEAR-FIELD MEASUREMENT - - - - - 30

 C. RESULTS FROM NEAR-FIELD MEASUREMENT - - - - 41

IV. CONCLUSION - - - - - 47

APPENDIX A: COMPUTER PROGRAM TO EVALUATE THE BEAM
 PATTERN OF A RANDOM NOISE SOURCE - - - - 50

LIST OF REFERENCES - - - - - 52

INITIAL DISTRIBUTION LIST - - - - - 53

LIST OF FIGURES

2.1	Angles and distances for the far field at Q from a source at Po - - - - -	13
3.1	Far field beam pattern measurement setup - - - -	29
3.2	Measured far field beam pattern - - - - -	31
3.3	Near field schematic representation of the position of the microphone - - - - -	32
3.4	Autocorrelation function measured at the boundary of the active region - - - - -	35
3.5	Autocorrelation function measured at the center of the speaker - - - - -	36
3.6	Near field experimental setup - - - - -	38
3.7	Frequency spectrum - - - - -	39
3.8	Predicted and measured beam pattern (UL = 5000 Hz, d = 12 cm, LL = 1100 Hz) - - - - -	43
3.9	Predicted and measured beam pattern (UL = 4250 Hz, d = 12 cm, LL = 1100 Hz) - - - - -	44
3.10	Predicted and measured beam pattern (UL = 4250 Hz, d = 15 cm, LL = 1100 Hz) - - - - -	45

I. INTRODUCTION

It has long been recognized that the best means of locating a deeply submerged submarine is by detecting the sound that it radiates into the water; also all surface ships are subject to attack by passive homing torpedoes and acoustic mines, both of which operate using the radiated noise of the ship. These facts make the far field radiated signatures a very important factor to determine detectability characteristics and capacity of survival in a hostile environment.

Free field measurement in the far field involves serious difficulties like ambient noise, multipath, convergence zone, attenuation, among others, which makes impracticable such kind of measurement. Instead a prediction of the Far Field using Near Field data is suggested. Certain general principles are repeatedly invoked in prediction. The first is that the vibratory powers of several sources is additive. This is based upon the assumption that the signals from any two sources are statistically uncorrelated, an assumption which is almost invariably found correct. Signal contributions from non-overlapping frequency bands are inherently uncorrelated; hence the total power over all frequencies is found by summing contributions from various frequency bands.

Several works have been done about prediction of Far Field beam pattern from Near Field measurements for discrete frequencies (Refs. 1,2,3,4). In general these methods deal

with the amplitude and phase information taken at the Near Field and the final result shows that the Fourier Transform of those measurements lead to the beam pattern. Consider the random noise as the random summation of sinusoidal waves, thus a complete analysis of the frequency bands can be achieved using a very narrow filter which center frequency can be shifted to cover all the spectrum, or a bank of narrow filters can be used. Adding the contribution of each frequency it should be possible to obtain the final beam pattern, but either procedure involves a tedious work, specially for broad band signals. There also remains the question of correlation between different bands.

The more general problem of predicting the Far Field noise beam pattern from a random noise source is of great practical importance. The theory of the noise field for systems that satisfy the wave equation has been developed by some investigators working in the fields of acoustics (Ref. 5), and optics (Ref. 6). Different methods had been suggested in order to generate a prediction in the far field, one of them consists of using correlation functions and the Green's function for the wave equation, for general time variations. This technique is used by Morse and Ingard (Ref. 7) in their book "Theoretical Acoustic," for describing non-periodic vibrations or random processes.

This paper discusses one possible method of Near Field analysis using the spatial correlation function and the Green's function which enables differential equations and

boundary conditions to be combined into an integral equation for the wave motion; the solution of the integral equation provides the intensity in the Far Field. This method could practically be used in collecting submarine radiated acoustic signatures.

II. GENERAL THEORY

The analysis of the disturbed region has to be done using a different approach than for discrete frequencies and one of the most common becomes the correlation technique. It is well known what the relationship is between the autocorrelation function of random signal and the total average power and the D.C. power contained in the signal. In a sense the autocorrelation function is a measure of time variation, spatial variation and statistical dependence in the region of inhomogeneities.

The study of the statistics of noise gives the possibility of finding the solution of the problem using the correlation function instead of a frequency decomposition and individual analysis of the frequency components in the random signal. In the process any phase information is lost, but the important point becomes the relation between the autocorrelation function and the field intensity, which is phase independent, and the angular dependence with respect to the acoustic axis of the source.

It is helpful to begin with a non periodical vibration problem, with several degrees of freedom, each degree of freedom has its own equation of motion and the general equation becomes:

$$M_n \frac{d^2 \vec{X}_n}{dt^2} = F_n(\vec{r}) + F'_n(\vec{r}, t) + D_n(\vec{v}, t) \quad (2.1)$$

$$n = 1, 2, \dots, N$$

where $F_n(\vec{r})$ is the internal force, $F'_n(\vec{r},t)$ is the external force, $D_n(\vec{v},t)$ is the frictional force, and M_n is the effective mass of the system.

Plotting the behavior of one component of x and its associated velocity on the Nth phase plane, it can be shown that the contour is not a closed-loop. Usually it will be a complicated non periodic curve confined within some limits given by the energy of the system but never repeating itself. Of course the N degree of freedom implies N different frequencies in such a way that the combination is not periodic. The displacement component will not be a periodic function of time, so the Fourier Analysis can not be applied. The average value of the displacement is also time dependent for short periods of time, but if the time is long enough the fluctuation can be evened out, and the resultant average becomes a constant; again it is necessary to use the statistical properties of the autocorrelation function, which is defined as follows:

$$R(\tau) = \lim_{T \rightarrow \infty} \left[\frac{1}{T} \int_{-\frac{1}{2}T}^{\frac{1}{2}T} x(t) \cdot x(t+\tau) dt \right] \quad (2.2)$$

The value of $R(0)$ is equal to the average power of the signal over the interval, and this will be the maximum value of $R(\tau)$. The size of " τ " is very important since the rapidity with which $R(\tau)$ drops to zero as τ is increased is a measure of the degree of randomness of the oscillation of the function. In the case of the spatial autocorrelation

function, the correlation distance, (d) , follows the same behavior.

The second step will be to study the radiation characteristic from a plane surface with randomly vibrating area, the goal in this section is to try to obtain a Green's function such that one or more parts of the resulting integral equation can be eliminated, and the remaining part easy enough to be integrated. The solution of this problem will be approached in four steps:

(1) Calculation of the far field due to a point source in the presence of a rigid boundary serves to outline the geometry and describe the role of the boundary and facilitate the choice of the right Green's function for subsequent steps.

(2) Calculation of the far field due to harmonic motion of parts of the surfaces itself which is assumed to have surfaces characteristic of a rigid boundary.

(3) Calculation of the far field due to harmonic motion of parts of the surfaces which have a particular acoustic impedance.

(4) Application of results from (3) to randomly vibrating area.

1. Consider sources in the presence of an infinite barrier like the arrangement shown in Figure 2.1. If the plane is perfectly rigid, the boundary condition is that the particle velocity and the gradient of the pressure at the surfaces is zero, thus, the effect of the boundary plane can be replaced by a set of images sources, symmetrically located with respect to the plane, both radiating into the region containing P_0 .

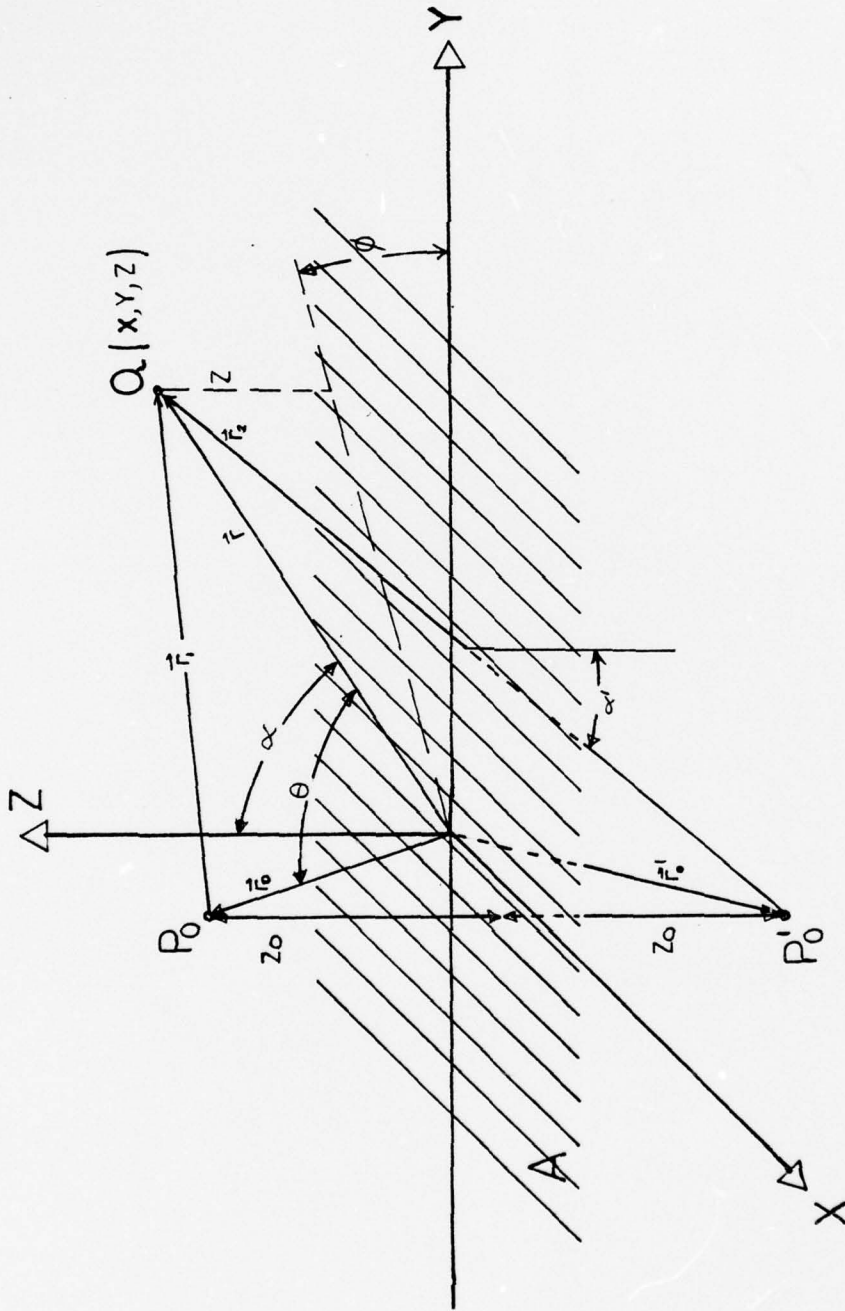


Figure 2.1 Angles and distances for the far field at Q from a source at P_0 .

The acoustic pressure at Q , defined by the vector \vec{r} , for a simple-harmonic source is then:

$$p = -i\rho c k S_{\omega} \left(\frac{1}{4\pi r_1} e^{ikr_1} + \frac{1}{4\pi r_2} e^{ikr_2} \right) e^{-i\omega t} \quad (2.3)$$

where k is the wave number and S_{ω} represent the strength of the source expressed in the frequency domain. Some approximations have to be made in Equation (2.3), assuming that Q is at a distance such that the two waves combine to form a source that looks like a single nonsimple source located at the origin. The magnitude of vectors \vec{r}_1 and \vec{r}_2 is defined by:

$$r_1 = |\vec{r} - \vec{r}_0| = r - \left(\frac{\vec{r}}{r}\right) \cdot \vec{r}_0 = r - r_0 \cos \theta$$

and

$$r_2 = |\vec{r} - \vec{r}'_0| = r + 2z_0 \cos \alpha - r_0 \cos \phi$$

Using these approximations Equation (2.3) becomes:

$$p \approx \frac{-i\rho c k}{2\pi r} S_{\omega} \cos(kz_0 \cos \alpha) e^{ik(r - r_0 \cos \theta + z_0 \cos \alpha)}$$

The distance from the source to the plane is an important parameter since it determines the constructive or destructive interference. For example, if kz_0 and kr_0 are

much less than l , the source is much smaller than a wavelength and the behavior of the pressure in the far field is very similar to that produced by a simple source of double strength of the original source. On the other hand, if z_0 is equal to a quarter wavelength the separation between the source and its image is one half the wavelength and its effect is a destructive interference. The same effect can be produced if instead of a point source a multipole source exists for which each point has its own image. Of course the boundary produces distortion in the near field which is not considered in this paper.

2. Now, considering that the sound waves in the bounded medium may be produced by the motion of the plane surface itself. With the plane rigid at z equal to zero, some portion of the plane may be moving in the z direction. For a simple harmonic motion $u_z = u_\omega \exp(-i\omega t)$, the boundary condition is that the gradient of the pressure is $ik\rho c u_\omega(x,y)\exp(-i\omega t)$, whereas, for the rest of the plane the partial derivative of the pressure with respect to z is zero.

The time independent part of the solution of the wave equation in terms of the Green's function is given by:

$$p_\omega(r) = \iiint f_\omega(r_0) G_\omega\left(\frac{r}{r_0}\right) dv_0 + \iint \left[G_\omega\left(\frac{r}{r_0}\right) \frac{\partial}{\partial n_0} p_\omega(r_0) - p_\omega(r_0) \frac{\partial}{\partial n_0} G_\omega\left(\frac{r}{r_0}\right) \right] dS_0 \quad (2.4)$$

since there are no sources in the medium the volume integral is equal to zero and the surface integral involves p and the outward pointing normal gradient at $z = 0$, but the description of the physical situation has specified only the normal gradient. The Green's function should be selected in such a way to eliminate the second part of the surface integral, keeping only the specified normal gradient of the pressure. The Green's function satisfying this requirement is given by:

$$G_{\omega}\left(\frac{\mathbf{r}}{r_0}\right) = \frac{1}{4\pi r_1} e^{ikr_1} + \frac{1}{4\pi r_2} e^{ikr_2}$$

in this case $r_1 = r_2$, because the source is in the surface boundary, thus, the bounded medium Green's function (G_{ω}) is twice as much as the unbounded medium Green's function g_{ω} , the reason is that each moving element of area radiates only into the half space $z > 0$, the source and its image have coalesced to form a source of double strength.

Applying this concept, Equation (2.4) becomes:

$$\begin{aligned} p_{\omega}(x,y,z) &= -ik\rho c \iint u_{\omega}(x_0,y_0) G_{\omega}\left(\frac{x,y,z}{x_0,y_0,z_0}\right) dx_0 dy_0 \quad (2.5) \\ &= -2ik\rho c \iint u_{\omega}(x_0,y_0) g_{\omega}\left(\frac{x,y,z}{x_0,y_0,0}\right) dx_0 dy_0 \end{aligned}$$

3. A perfectly rigid boundary is unrealizable. The common situation is that the boundary has a particular acoustical impedance defined by its density and the velocity

of sound in the medium. Then, the boundary reacts to an incident pressure and every portion of the plane is moving, and a different method has to be applied in order to distinguish the active regions in the plane, where energy is fed into the medium from the passive areas.

For the passive areas the relationship between p and its normal derivative is given by:

$$-u_z = -\frac{1}{ik\rho c} \cdot \frac{\partial p}{\partial z} = \frac{\beta}{\rho c} p \quad \text{at } z = 0 \quad (2.6)$$

where β is the impedance ratio between the impedance of the medium where sound propagates and the impedance of the surface boundary. For the Active Areas the normal fluid velocity, plus the admittance of the boundary times the pressure at $z = 0$ must differ from zero, this difference will be defined as the driving velocity (u_ω)

$$\left(u_z + \frac{\beta}{\rho c} p\right)_{z=0} = \left(\frac{1}{ik\rho c} \frac{\partial p}{\partial z} + \frac{\beta}{\rho c} p\right)_{z=0} = u_\omega e^{-i\omega t} \quad (2.7)$$

To simplify the surface integral, the Green's function could be arranged such that the surface integral over the passive areas is zero. This is accomplished by a Green's function that satisfies:

$$\frac{\partial G_\omega}{\partial z_0} = -ik\beta G_\omega \quad (2.8)$$

The integral over the active area is:

$$p_{\omega} = - \iint \left(\frac{\partial p}{\partial z_0} G_{\omega} - p_{\omega} \frac{\partial G_{\omega}}{\partial z_0} \right)_{z=0} dx_0 dy_0 \quad (2.9)$$

Using Eq. (2.8) in Eq. (2.9)

$$p_{\omega} = - \iint \left[\frac{\partial p_{\omega}}{\partial z_0} + ik\beta p_{\omega} \right] G_{\omega} dx_0 dy_0 \quad (2.10)$$

The expression in parentheses is the driving velocity in the active region given by (2.7), thus Eq. (2.10) becomes:

$$p_{\omega} = -ik\rho c \iint u_{\omega}(x_0, y_0) G_{\omega} \left(\frac{x_0, y_0, z}{x_0, y_0, 0} \right) dx_0 dy_0 \quad (2.11)$$

which has the same form as Equation (2.5), but this time an exact representation of the Green's function as was stated previously is not possible. However, a good approximation valid when the measurement point Q is not closer than a half wavelength to the boundary surface and which satisfy Equation (2.8) is given by:

$$G_{\omega} \approx \frac{e^{-ikr_1}}{4\pi r_1} + \left[\frac{\cos \alpha' - \beta}{\cos \alpha' + \beta} \right] \cdot \frac{e^{-ikr_2}}{4\pi r_2} \quad (2.12)$$

where the variables correspond to Fig. 2.1. Although this form of the Green's function is derived for the problem of a volume source in the presence of a non-rigid boundary, it may be used since it accomplishes the simplification of the problem in hand. [In this approximation there is an image

at P'_0 , but the wave it radiates has an amplitude which depends on the angle α' which the line r_2 makes with the z-axis normal to the boundary. The ray of acoustic radiation which reaches the point Q from the source point at P_0 by reflection, strikes the reflecting surface at Q at an angle α' of incidence and reflection. The wave which goes directly from P_0 to Q without reflection, given by the first term, is independent of the inclination of r_1 ; the reflected wave, given by the second term, depends on the angle of reflection. The factor β introduced the variation in the reflected sound due to the boundary. In this way the term in parentheses represents the reflection coefficient.]

In the far field Eq. (2.12) can be simplified using $r_1 = r_2$:

$$G_\omega = \frac{e^{ikr_1}}{4\pi r_1} \left[1 + \frac{\cos \alpha' - \beta}{\cos \alpha' + \beta} \right] = \frac{e^{ikr_1}}{2\pi r_1} \left[\frac{\cos \alpha'}{\cos \alpha' + \beta} \right] \quad (2.13)$$

From Eqs. (2.11) and (2.13) the pressure in the far field is given by:

$$p_\omega = \frac{-ik\rho c}{2\pi} \iint u_\omega(x_0, y_0) \frac{\cos \alpha'}{\cos \alpha' + \beta} \frac{e^{ikr_1}}{r_1} dx_0 dy_0 \quad (2.14)$$

Observe that the integral is over the active region of the plane which is assumed to be confined to the circle of radius "a" about the origin.

In the far field the last equation can be simplified neglecting terms of order a/r and smaller and using the approximation $\cos \alpha' = \cos \alpha = z/r$,

$$r_1 \approx r - (x_0 \cos \phi + y_0 \sin \phi) \sin \alpha$$

$$\frac{1}{r_1} \approx \frac{1}{r} \quad \text{and} \quad \tan \phi \approx \frac{y}{x}$$

Thus, Equation (2.7) becomes:

$$p_\omega(\vec{r}) \approx -ik\rho c \frac{\cos \alpha}{\beta + \cos \alpha} \cdot \frac{e^{ikr}}{2\pi r} \iint u_\omega(x_0, y_0) e^{-i\vec{k} \cdot \vec{W}_0 \sin \alpha} dx_0 dy_0 \quad (2.15)$$

where the vector \vec{W}_0 lies in the xy plane, with x_0 , y_0 as component; and vector k has the \vec{r} direction whose components are:

$$\begin{aligned} k_x &= k \cos \phi \sin \alpha \\ k_y &= k \sin \phi \sin \alpha \\ k_z &= k \cos \alpha \end{aligned}$$

A close study of the integral part of Equation (2.15) shows that the angular distribution of the Far Field is proportional to the two dimensional Fourier Transform of the distribution of the driving velocity in the active region, which is defined by:

$$U_{\omega}(k_x, k_y) = \frac{1}{4\pi^2} \iint_{-\infty}^{\infty} u_{\omega}(x_0, y_0) e^{-k_x x_0 - k_y y_0} dx_0 dy_0$$

$$u_{\omega}(x_0, y_0) = \iint_{-\infty}^{\infty} U_{\omega}(k_x, k_y) e^{ik_x x_0 + k_y y_0} dk_x dk_y$$

$$f_{\omega}(\alpha, \phi) = \frac{8\pi^2 \cos \alpha}{\beta + \cos \alpha} U_{\omega}(k \cos \phi \sin \alpha, k \sin \phi \sin \alpha) \quad (2.16)$$

Thus Equation (2.15) takes the form:

$$P_{\omega}(r) \approx -ik\rho c \frac{e^{ikr}}{4\pi r} f_{\omega}(\alpha, \phi) \quad (2.17)$$

The angular dependence is given by the factor f_{ω} , which measures the relative amplitude of the pressure with respect to the center of the active region.

Several properties of the Far Field can be studied. If the coordinate axes are rotated to X_0, Y_0 , such that X_0 axis is the intersection of the rz plane, the appropriate transformation is given by:

$$x_0 = X_0 \cos \phi - Y_0 \sin \phi$$

$$y_0 = X_0 \sin \phi + Y_0 \cos \phi$$

Under this transformation the time independent particle velocity becomes:

$$U_{\omega}(k \cos \phi \sin \alpha, k \sin \phi \sin \alpha) = \frac{1}{4\pi^2} \int e^{-ikX_0 \sin \alpha} dX_0 \int u_{\omega}(X_0, Y_0) dY_0$$

This equation shows the one dimensional Fourier transformation in the X_0 direction, of the average:

$$u_{\phi}(\omega, X_0) = \frac{1}{2\pi} \int u_{\omega}(X_0, Y_0) dY_0$$

of the particle velocity $u_{\omega}(X_0, Y_0)$ in the Y_0 direction.

It can also be observed that $u_{\phi}(\omega, X_0)$ is a function of X_0 , the distance in the direction of the measured point Q; it is also a function of ϕ , the direction of the rz plane, and of the frequency $\omega/2\pi$.

If the particle velocity $u_z(x, y, t)$ is an arbitrary function of space and time and $u_{\omega}(x, y)$ is its time dimension Fourier transform, then the pressure field at a point Q (r, α, ϕ) is the inverse transform of P_{ω} given by Equation (2.17)

$$p(r, t) = \frac{\rho}{4\pi r} \int_{-\infty}^{\infty} f_{\omega}(\alpha, \phi) e^{-i\omega(t - \frac{r}{c})} d\omega \quad (2.18)$$

Now, applying the rotation of axes as defined before, Equation (2.18) can be expressed as:

$$p(r, t) = \frac{\rho}{2\pi r} \cdot \frac{\cos \alpha}{\beta + \cos \alpha} \int_{-\infty}^{\infty} -i\omega e^{-i\omega(t - \frac{r}{c})} d\omega \int_{-\infty}^{\infty} e^{i(\frac{\omega}{c})X_0 \sin \alpha} dX_0$$

$$\times \int_{-\infty}^{\infty} dY_0 \frac{1}{2\pi} \int_{-\infty}^{\infty} e^{i\omega Z} u(X_0, Y_0, Z) dZ \quad (2.19)$$

$$p(r, t) = \frac{\rho}{2\pi r} \cdot \frac{\cos \alpha}{\beta + \cos \alpha} \frac{\partial}{\partial t} \left[\int dX_0 \int dY_0 u(X_0, Y_0, t + \frac{1}{c} X_0 \sin \alpha - \frac{r}{c}) \right]$$

This equation shows clearly some of the properties of the Far Field. An appropriate summation of the normal acceleration of the active area gives the total field at the point of interest. Also the contribution to the pressure at r , at time t , from the line X_0 , $-\infty < Y_0 < \infty$, depends on the normal acceleration on the line at time $t + (1/c)X_0 \sin(\alpha) - r/c$, at time $r/c - (X_0/c) \sin(\alpha)$ earlier, which is the time required for the sound to travel from the line to point Q .

4. All the formulae developed so far can be used to compute the mean intensity at r, α, ϕ , produced by an area A of the boundary which is vibrating with a random distribution of velocity. The particle velocity in the active area A is a function of position as well as of time. In this regard, it becomes a random variable and a way to describe its behavior is using its statistical properties. In this particular case the autocorrelation function is used as a means to describe the behavior of the random source. Considering the particle velocity as a function of position and time in the active area, the autocorrelation function is defined by:

$$R(\xi, \eta, \tau) = \frac{1}{AT} \iiint u_z^*(x, y, t) u_z(x + \xi, y + \eta, t + \tau) dx dy dt$$

where the integration is over the active area A , and T is over a long interval of time. Also the Fourier transform of the velocity is given by:

$$U_{\omega}(k_x, k_y) = \frac{1}{8\pi^3} \iiint u_z(x, y, t) e^{i\omega t - ik_x x - ik_y y} dx dy dt .$$

From this equation the space time spectrum level of the particle velocity is:

$$|U_{\omega}|^2 = \frac{AT}{64\pi^6} \iiint_{-\infty}^{\infty} R(\xi, \eta, \tau) e^{i\omega\tau - ik_x \xi - ik_y \eta} d\xi d\eta d\tau \quad (2.20)$$

In the far field it is known that the intensity is given by the real part of the pressure times the particle velocity, but also the velocity is related to pressure for the relation $u = p/\rho c$, thus using Eq. (2.16) and Eq. (2.17):

$$\left| \frac{p}{\rho c} \right|^2 \approx \frac{\rho c}{r^2} \frac{4\pi^2 k^2 \cos^2 \alpha}{|\beta + \cos \alpha|^2} |U_{\omega}(k \sin \alpha \cos \phi, k \sin \alpha \sin \phi)|^2 \quad (2.21)$$

This equation is related to the autocorrelation function by Equation (2.20). The problem is now reduced to getting the form of $R(\xi, \eta, \tau)$ in space and time. A reasonable assumption could be a Gaussian waveform where the value of R falls off smoothly as its arguments are increased.

Assume that the autocorrelation is given by:

$$R(\xi, \eta, \tau) = |U_0|^2 e^{-\frac{1}{2d^2} (\xi^2 + \eta^2) - \frac{1}{2} (\omega_n \tau)^2} \quad (2.22)$$

where U_0^2 is the mean square particle velocity of the active area averaged over time interval T ; d stands for the correlation distance along the plane, ω_n is the upper

angular frequency limit of the spectrum, which also can give the correlation time, and the lower limit of the wavelength.

Using this value of the autocorrelation function and equations (2.20) and (2.21), the intensity field was evaluated:

$$I_r(\omega) \approx \rho c \frac{AT}{r^2} (2\pi)^{-5/2} \frac{\omega^2 d^2 |U_0|^2 \cos^2 \alpha}{c^2 \omega_n |\beta + \cos \alpha|^2} e^{-\frac{1}{2}(\frac{\omega d}{c})^2 \sin^2 \alpha - \frac{1}{2}(\frac{\omega}{\omega_n})^2} \quad (2.23)$$

But this is only for a specific frequency; in order to get the total field intensity it would be necessary to consider the contribution of all the frequency components of the random signal. A logical way to accomplish this is to integrate Equation (2.23) with respect to frequency. Note that the integrand has a maximum when the exponent is zero at:

$$\omega = 2^{1/2} \omega_n (1 + k_n^2 d^2 \sin^2 \alpha)^{1/2}$$

$$I_r(r) = \frac{2\pi}{T} \int_{-\infty}^{\infty} I_r(\omega) d\omega \approx \rho c \frac{A}{2\pi r^2} \cdot \frac{|U_0|^2 \cos^2 \alpha}{|\beta + \cos \alpha|^2} \cdot \frac{(k_n d)^2}{[1 + (k_n d)^2 \sin^2 \alpha]^{3/2}} \quad (2.24)$$

A simple analysis of this formula shows that the intensity is proportional to the impedance of the medium,

times the mean square particle velocity in the active area, times the ratio between the active area, A , and the area of the half sphere of radius r , times an angle distribution function, which depends on the maximum frequency of the spectrum (inverse of the correlation time), the speed of sound and the correlation distance, d .

Trying to apply this theory to practical cases, two main problems arose. The first is that in real situations the frequency spectrum is band limited, usually due to the physical characteristics of the source. Under this consideration the limit of integration should have an upper bound (UL) and a lower limit (LL), in this form, Equation (2.23) becomes:

$$I_r(r) = 2\rho c \frac{AT}{r^2} (2\pi)^{-5/2} \frac{d^2 |U_o|^2 \cos^2 \alpha}{c^2 \omega_n |\beta + \cos \alpha|^2} \cdot \frac{2\pi}{T} \int_{LL}^{UL} \omega^2 e^{-\frac{1}{2}(\frac{\omega d}{c})^2 \sin^2 \alpha - \frac{1}{2}(\frac{\omega}{\omega_n})^2} d\omega \quad (2.25)$$

There is no analytical solution for this equation, so a numerical method of integration had to be used in order to get the intensity in the Far Field.

The second problem is the difficulty in measuring the autocorrelation function of the randomly vibrating area, which is related to the particle velocity in the active area. Instead it can be assumed that if the area close to the active region is vibrating with similar characteristics, then the impedance ratio becomes unity and the autocorrelation

in the Near Field gives the mean square particle velocity;

Equation (2.25) becomes:

$$I_r(r) = 2\rho c \frac{A}{r^2} (2\pi)^{-3/2} \frac{d^2 |U_0|^2 \cos^2 \alpha}{c^2 \omega_n |1 + \cos \alpha|^2} \int_{LL}^{UL} \omega^2 e^{-\frac{1}{2}(\frac{\omega d}{c})^2 \sin^2 \alpha - \frac{1}{2}(\frac{\omega}{\omega_n})^2} d\omega \quad (2.26)$$

This equation is angle dependent, thus the intensity in the Far Field depends on the angular position with respect to the acoustical axis. In this way it is possible to evaluate the beam pattern. Observe also that ω_n should lay inside of the limit of integration or at least equal to the upper limit, otherwise the process would show a discontinuity which is not possible because the frequencies contributing to the field are given by the limit of integration.

III. EXPERIMENTAL RESULTS USING THE PLANE MODEL

To validate the theoretical model described in Section II, Far Field and Near Field measurements were made on a horn speaker in an anechoic chamber. The actual beam pattern in the far field of the horn-speaker was taken and also the autocorrelation function in different points of the near field were obtained in order to get the mean square particle velocity in the Near-Field and be able to predict the Far Field Beam Pattern.

A. FAR-FIELD MEASUREMENT

The normalized Far Field beam pattern was obtained using the experimental set up shown in Figure 3.1. Since the source was driven by random noise the distance of the near field is variable. The criterion for near field is usually given for one particular frequency, as the frequency is made lower and lower the near field also decreases and eventually disappears for practical purposes. That is the reason for the presence of the high pass filter which limits the low frequency component to 1300 Hz in order to get an appreciable near field region. This is necessary for obtaining far field and near field measurements under the same frequency spectrum. The signal is then amplified and applied to the horn speaker. The microphone was placed in the far field at a distance of 5.8 meters from the source, the received signal was amplified

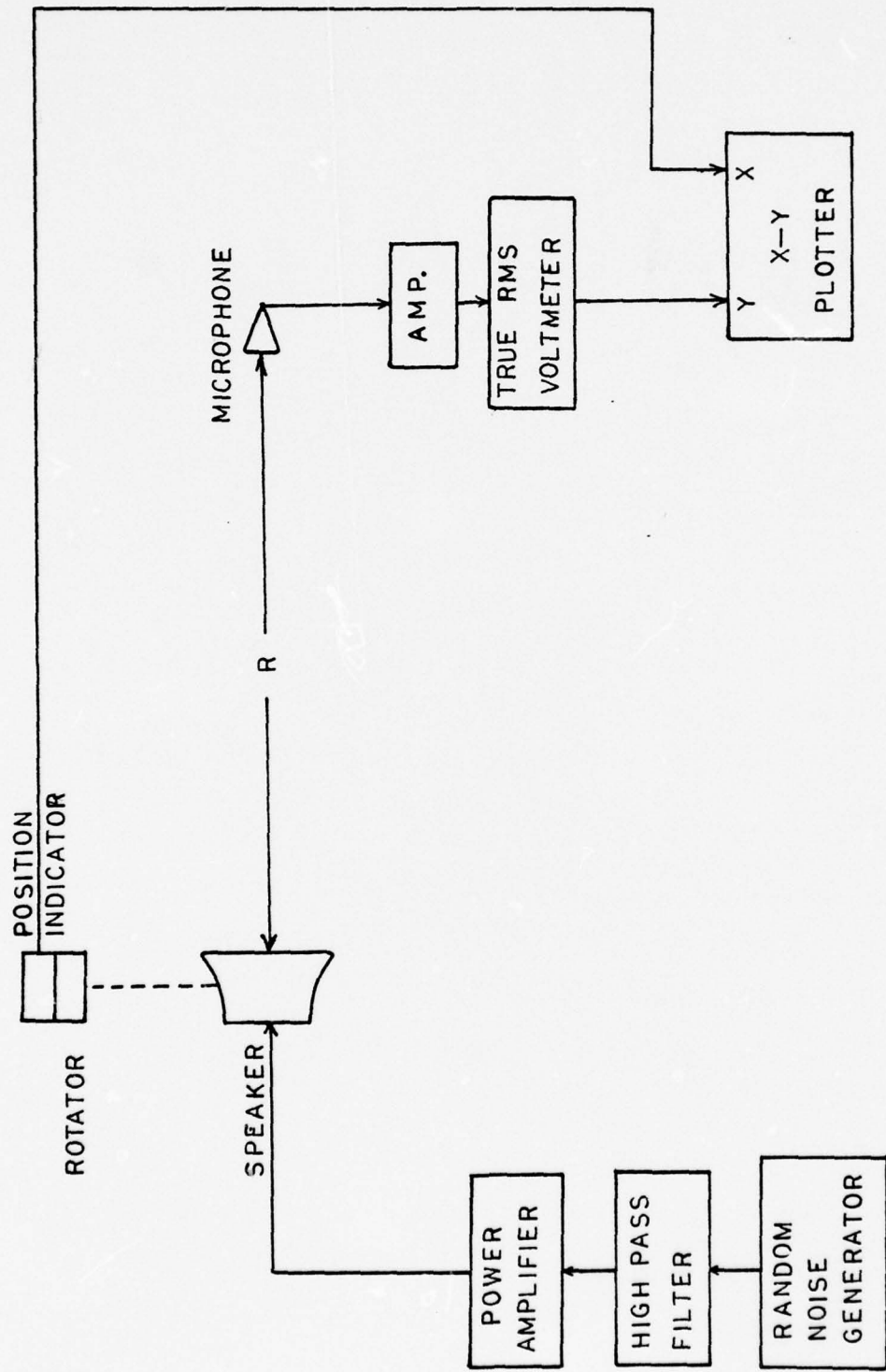


Figure 3.1 Far field beam pattern measurement setup.

and the output connected to a true RMS Voltmeter which also generates a DC voltage output proportional to the deflection of the needle for the selected scale, this voltage was applied to the Y axis of the plotter. The X axis of the plotter received information from the position indicator as a DC voltage proportional to the angular displacement of the acoustic axis of the horn speaker. The normalized pressure amplitude versus angular position is shown in Figure 3.2.

This was the actual Far Field Beam Pattern which had to be compared with the beam pattern evaluated using the mathematical model described in the previous section.

B. NEAR-FIELD MEASUREMENT

The intensity in the Far Field, as defined by Equation (2.26) depends, among other factors, upon the mean square particle velocity. The mean square particle velocity is a source quantity which was shown to be related to the autocorrelation function. The evaluation of the factor is possible by using an array of microphones over the entire active region and the summation of the received signal fed into the correlator. The microphone array was not available, instead a single microphone was used to take a measurement each 5 cm in the vertical and horizontal direction trying to cover the active area as shown in Figure 3.3. The autocorrelation values obtained at each single point is then averaged and the resultant value was used to describe the mean square particle velocity.

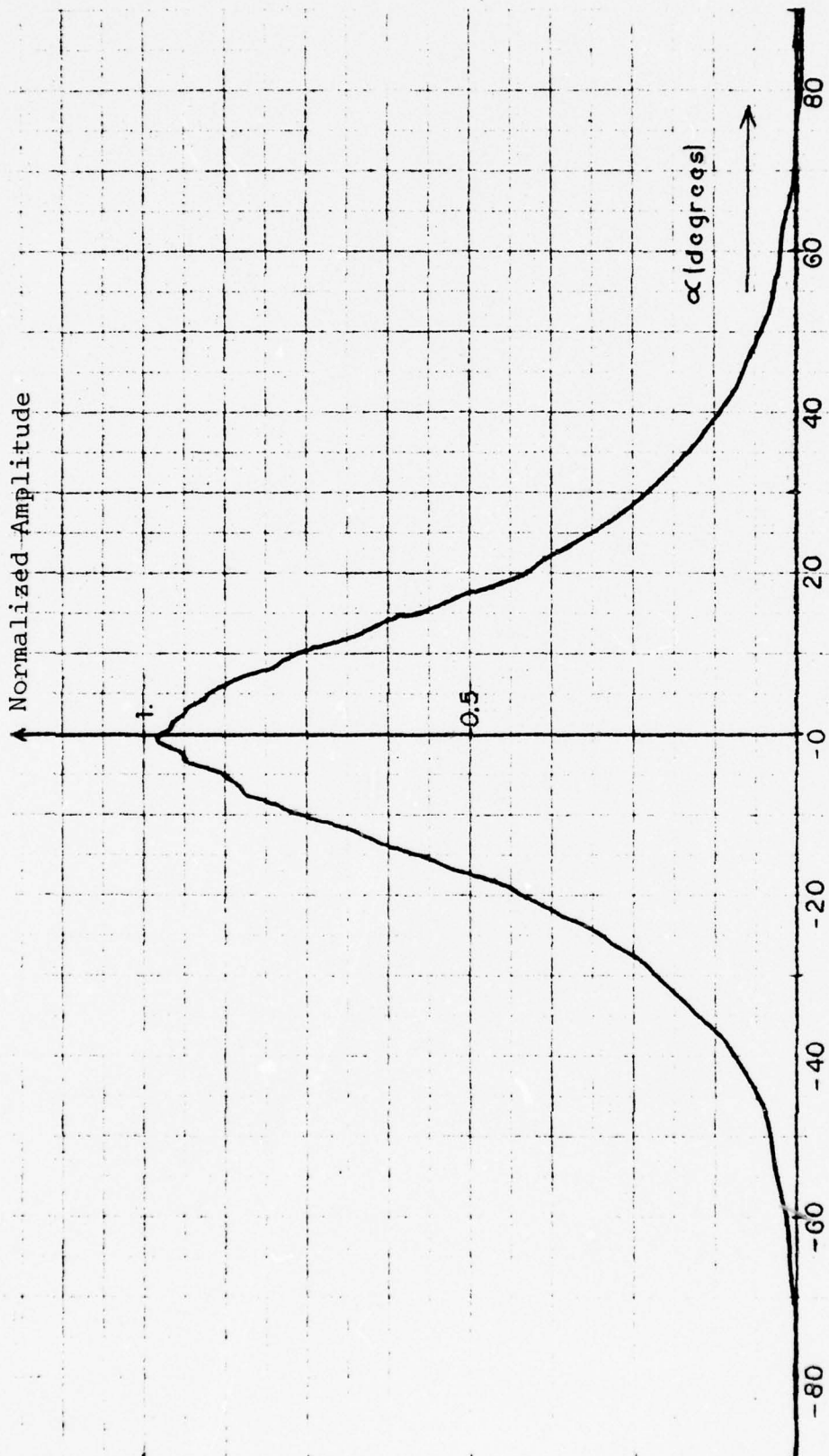


Figure 3.2 Measured far field beam pattern. Horn Speaker.

$L = 5 \text{ cm.}$

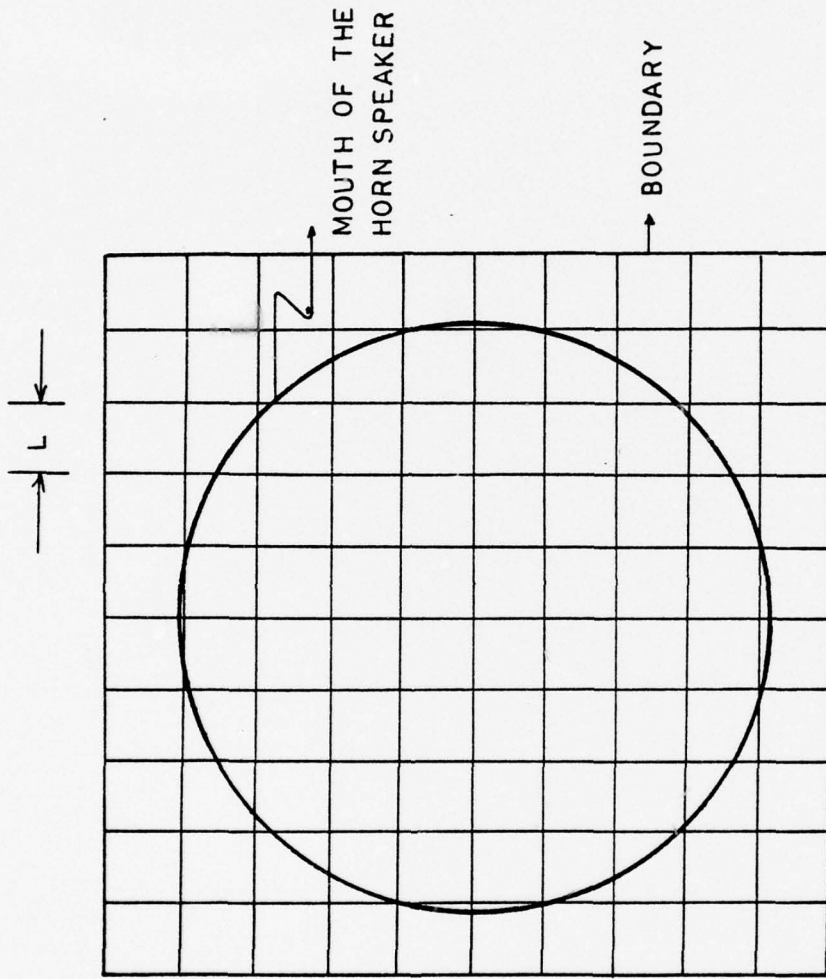


Figure 3.3 Near field schematic representation of the position of the microphone. (View facing horn)

The correlator was a SAICOR model SAI-43A, which was used in the autocorrelation mode, the function is determined simultaneously at 400 incremental lag points, the completed correlation function is displayed at one time, the function is provided with incremental lag or time delay value ranging from 0.2 microseconds to 1 sec resulting in total time delays from 80 microseconds to 400 sec. Precomputation delay of 800 lag values selected in 200 lag increments allows the autocorrelation function to be viewed symmetrically about zero or up to 800 lag values removed from zero. The averaging is accomplished digitally in a linear fashion with fixed summations ranging from 2^9 to 2^{17} in binary steps. The quantization is 8 bits per channel.

The SAI-43 operates as follows: one input signal is applied to either channel, and internally routed to the second channel, the signal is sampled at the rate indicated by the operator-selected sample increment and then is quantized in both channels. Channel I is the channel which contains the 400 word memory. Channel II contains the one word memory - the present sample. At the time called "Present Time", the correlator performs the multiplication of the present value word of Channel II by each of the 400 words in Channel I. The product "0" times "0" becomes an entry in $R(0)$, the first point of the autocorrelation function the product "0" times "1" becomes an entry for $R(1)$ and finally "0" times "399" becomes an entry for $R(399)$. At the end of this arithmetic cycle the correlator has performed one calculation for each so-called bin of the autocorrelation function.

The product in $R(0)$ is the first entry for the zero-lag autocorrelation value, while the product in $R(399)$ is the first entry for the correlation value at a lag in Channel I equal to $399t$. These first entries, resulting from one sample in Channel II are expanded to the full correlation function by taking repeatedly updated value of the sample in Channel II and correspondingly updated values in Channel I and then averaged. In effect the 400 word memory slides ahead one word and the arithmetic cycle begins again. For all t increments that are equal or longer than 500 usec the SAI-43A is said to operate in real time. But for increments less than 500 usec the figure is different. Assume an increment less than 50 msec, it could have completed eight cycles in 400 msec instead of one, therefore it is eight times slower than the real time instrument.

The output of the correlator can be displayed in an oscilloscope or in an x-y plotter, the voltage output in the autocorrelation mode can be determined by the following formula:

$$R(v^2) = \frac{x(\text{VOLT})}{125} (10)^{\text{dBA}/10} \quad (3.1)$$

where x is the voltage as seen as the output of the SAI-43A dBA is the dB setting of the input channel. R is the correlation value in $(\text{volt})^2$ to be determined.

For illustration purposes Figure 3.4 and Figure 3.5 show the autocorrelation function, $R(0,0,0)$, for the point of maximum intensity, (center of the speaker), and the point of

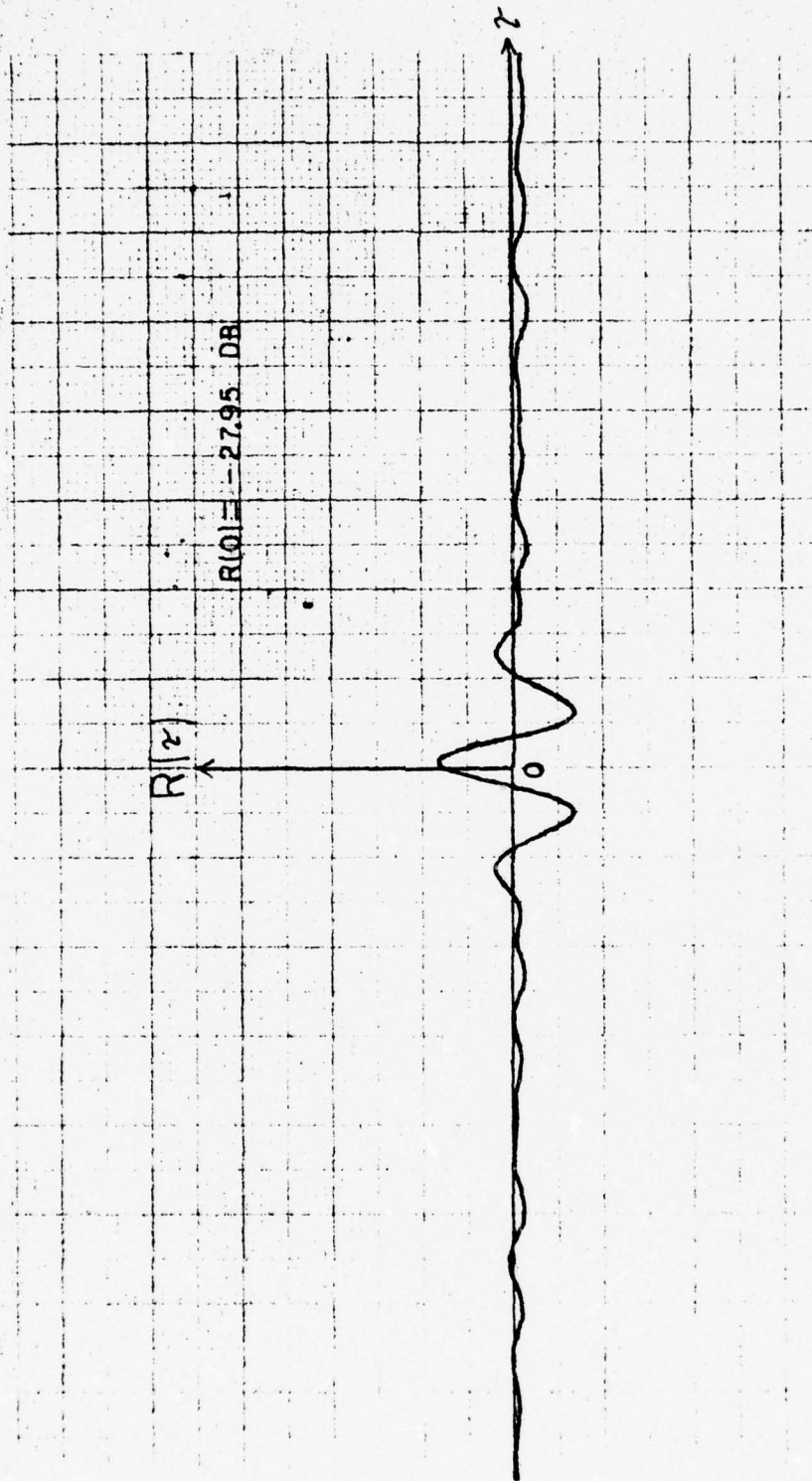


Figure 3.4 Autocorrelation function measured at the boundary of the active region

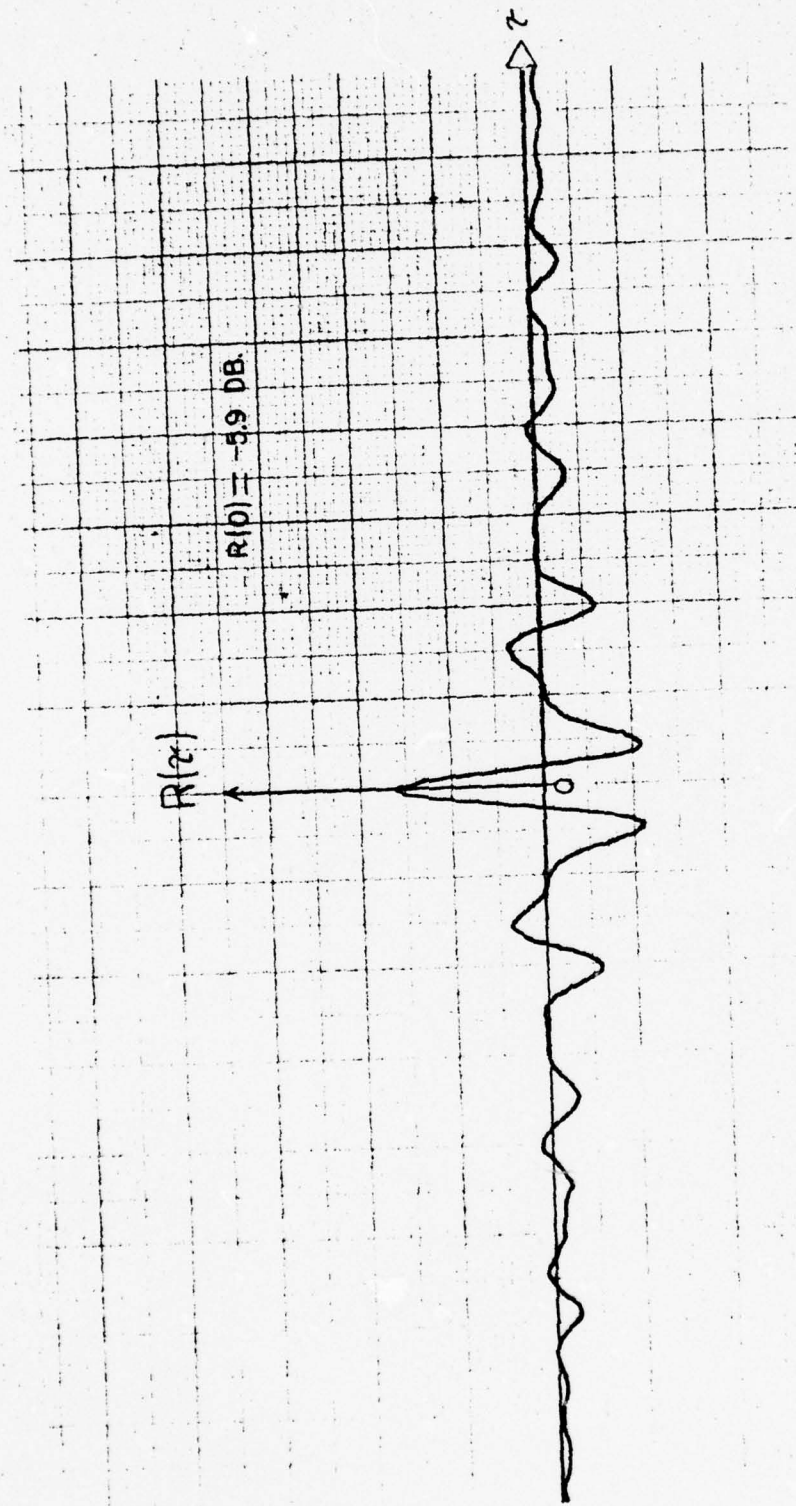


Figure 3.5 Autocorrelation function measured at the center of the speaker

minimum intensity, which correspond to the corner of the boundary of the active region, the relative power between them is more than 20 dB.

The physical arrangement in the anechoic chamber and the instrumentation for taking the autocorrelation function at each point in the near field is shown in Figure 3.6. The autocorrelation of the band limited noise becomes the $\sin x/x$ function, the amplitude of the function is variable depending on the position of the microphone. As described before it is also possible to get the power at each point of the autocorrelation function.

The criteria used for determining the active area was on the basis of the differences in power between the center of the horn up to the point which had 20 dB less power, which corresponds to the boundary of the active area shown in Figure 3.3.

The other important measurement was the frequency spectrum of the received signal which is given in Figure 3.7. This was obtained using the basic setup but with a wave analyzer instead of the correlator. The frequency sweep was made very slow in order to get a good average. The main use of this figure was to provide the proper limits of integration for Equation (2.26). The limit of integration became a quite important parameter since it modifies greatly the form of the normalized beam pattern; thinking in terms of a transducer, it is known that higher frequencies make the beam narrower and the low frequencies have a wider beam, so looking at

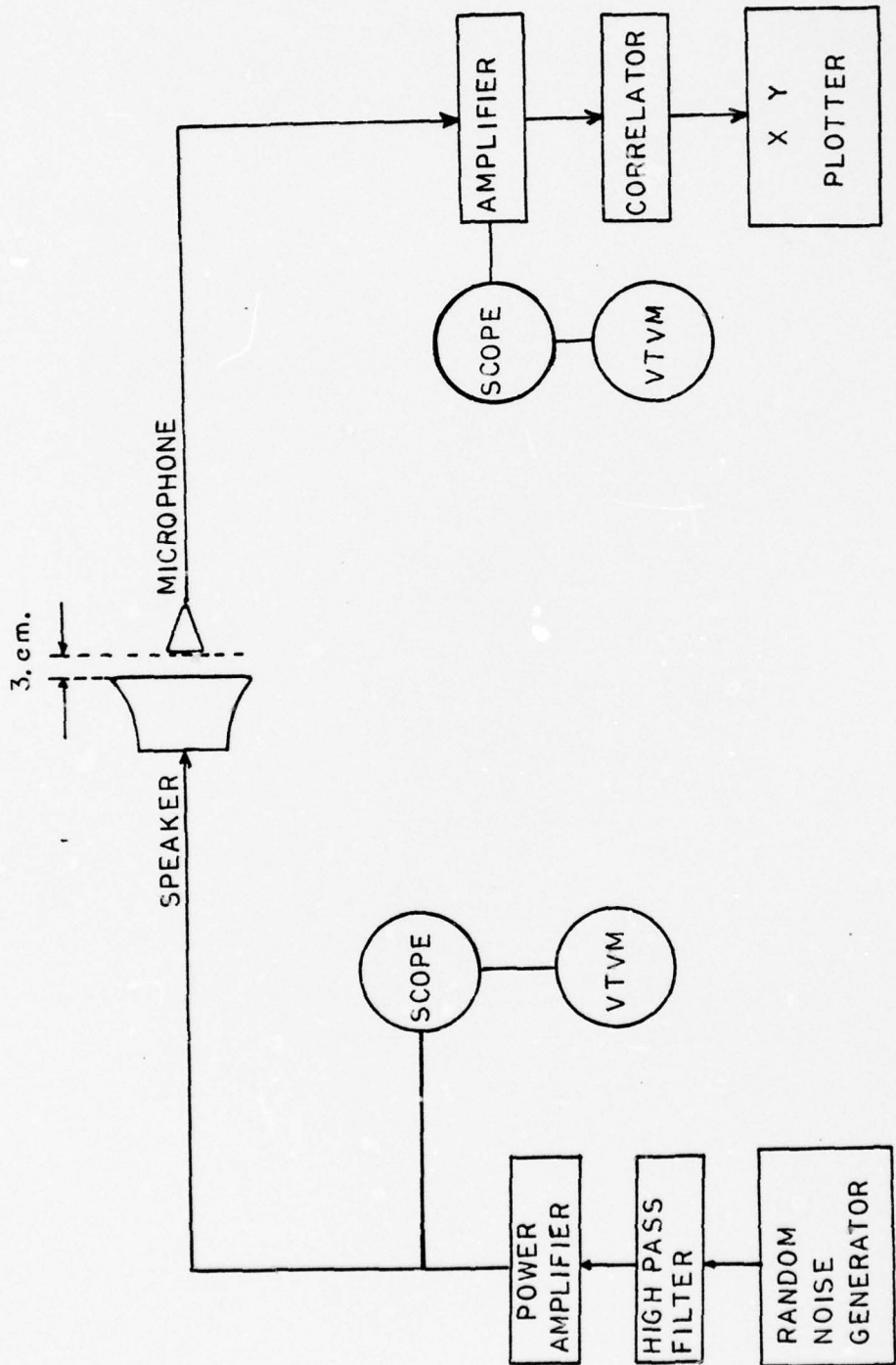


Figure 3.6 Near field experimental setup.

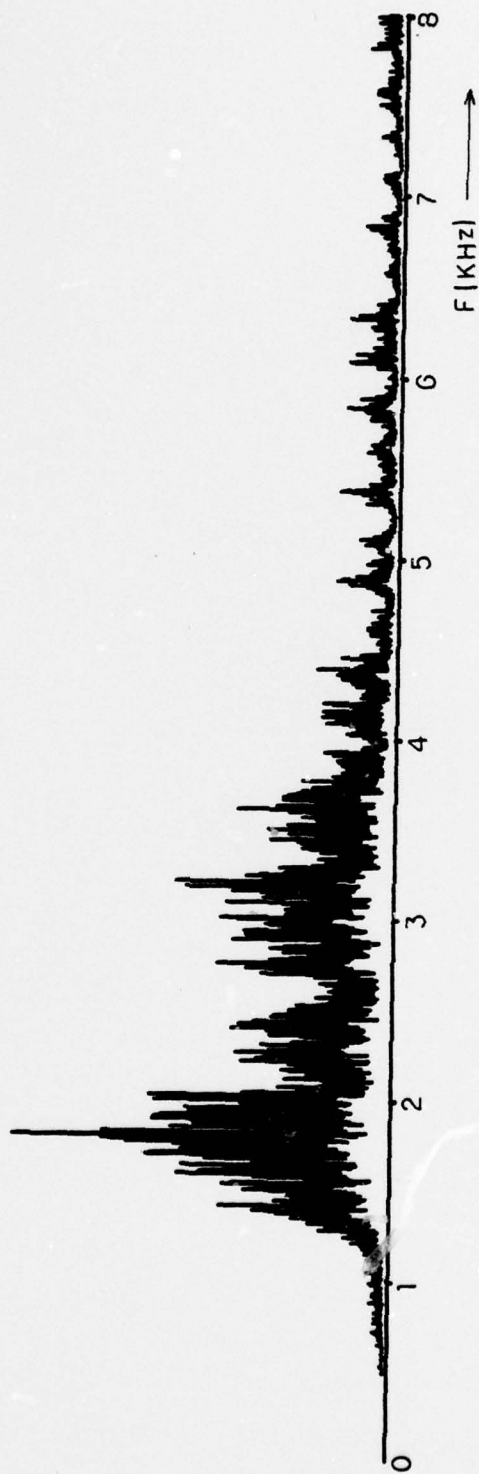


Figure 3.7 Frequency spectrum. Horn Speaker.

Figure 3.2, the actual beam pattern, it is logical to assume that the main contributions are given by the low frequencies, and that is exactly what the Frequency Spectrum shows in Figure 3.7. The lower limit of integration is assumed to be 1100 Hz and the upper limit is 5000 Hz, the contributions of the other frequencies was small; this also showed that the speaker has a low frequency response, although it covers the important band of the human hearing.

Another critical factor in the Near-Field measurements was the correlation distance, since its effect in the width of the beam is great. The symmetry of the source caused some difficulties; it was found that all points located at the same distance from the axis of the horn had a very good correlation, regardless of the distance between them, but along the same angular position a distance of 12 cm was enough to diminish greatly the spatial autocorrelation function. This suggested that the correlation distance for this experiment is a vectorial parameter, but was used like a scalar along this work. It is useful to point out that in a real situation with an asymmetric source driven by several sources with different frequency bands, like a submarine in which each section is affected for different set of frequencies and also the physical configuration changing in space, the autocorrelation distance has to be easy to measure experimentally and its vectorial characteristic should disappear leading to a scalar parameter. Otherwise the pattern must be built up from several sources.

Along this experiment a correlation distance of 12 cm was used.

C. RESULTS FROM NEAR-FIELD MEASUREMENT

The first step in the data processing was to get the average mean square particle velocity. Using the data collected in the experiment and the formula given by Equation (3.1) it was possible to evaluate the power at each point of the active area, this power was averaged, the entire process was done using an IBM-360 computer program in fortran IV language. The value obtained in this program represents the mean square of the particle velocity expressed by the Equation (2.22), where the value of the autocorrelation function is at zero spatial and time shift.

The approximation used for that evaluation was, of course, an additional source of inaccuracy in the experiment, but should not affect too much the final result, because what is really affected is the intensity field. The normalized beam pattern is practically unaffected since the relative power between each angular position was the subject of interest. In the case of trying to obtain a radiation pattern, which is beyond the scope of this work, then U_0^2 becomes a very important factor since it affects the Power Level of the signal.

The solution of Equation (2.26) is the actual prediction of the Far Field Beam Pattern. Again the computer system was used for performing numerical integration, a library sub-routine called DQATR was used. It was necessary to use

double precision in order to obtain a reasonable accuracy. The sub-routine uses the trapezoidal rule in connection with Rombergs principles for evaluating the approximation of the integral value of the function.

The resulting computed Far-Field is shown in Figure 3.8 in comparison with the actual Far-Field. Note that the agreement between the predicted and the measured beam pattern is fair in shape but slightly out in values, the actual beam pattern shows a wider beam than the predicted one. Several factors can produce that difference, the correlation distance could be one of the main factors due to its specially variable characteristic in this experiment, as it was explained before. Also the limits of integration assumed an important role, strong high frequency components could produce that narrow beam.

In order to study the variation of the function with respect to the limits of integration more calculations were made reducing the upper limit to 4250 Hz, all other parameters were kept constant. The result of this calculation is shown in Figure 3.9. This time a better agreement was obtained between the actual and the predicted beam patterns. A wider beam was obtained but still showed a small difference with the actual beam pattern.

The effect of the correlation distance is shown in Figure 3.10. The limits of integration were kept at 4250 Hz and 1100 Hz, and the correlation distance was increased to 15 cm in the calculation. It can be seen that a small variation in

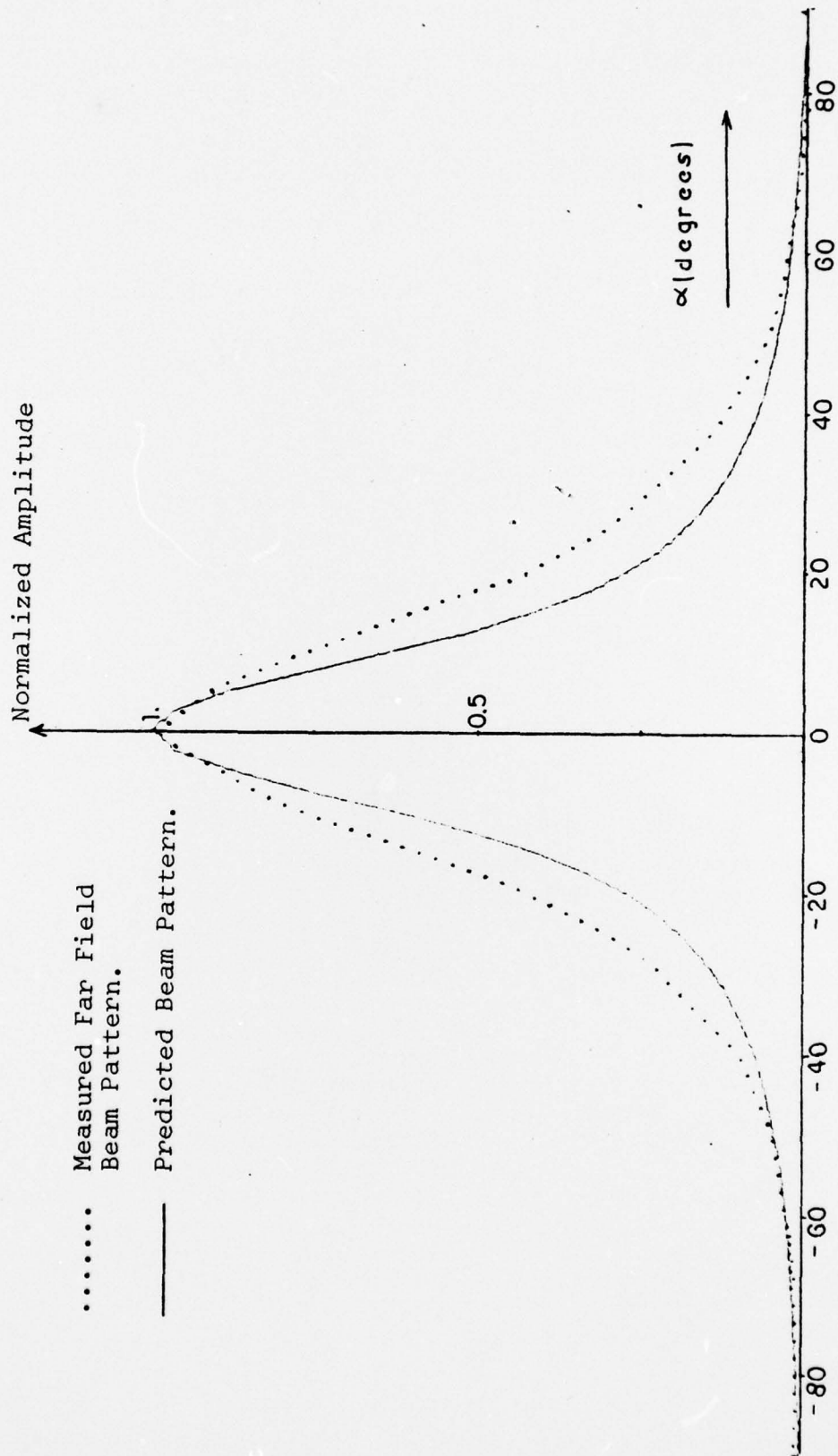


Figure 3.8 Predicted and measured beam pattern
(UL = 5000 Hz, d = 12 cm, LL = 1100 Hz).

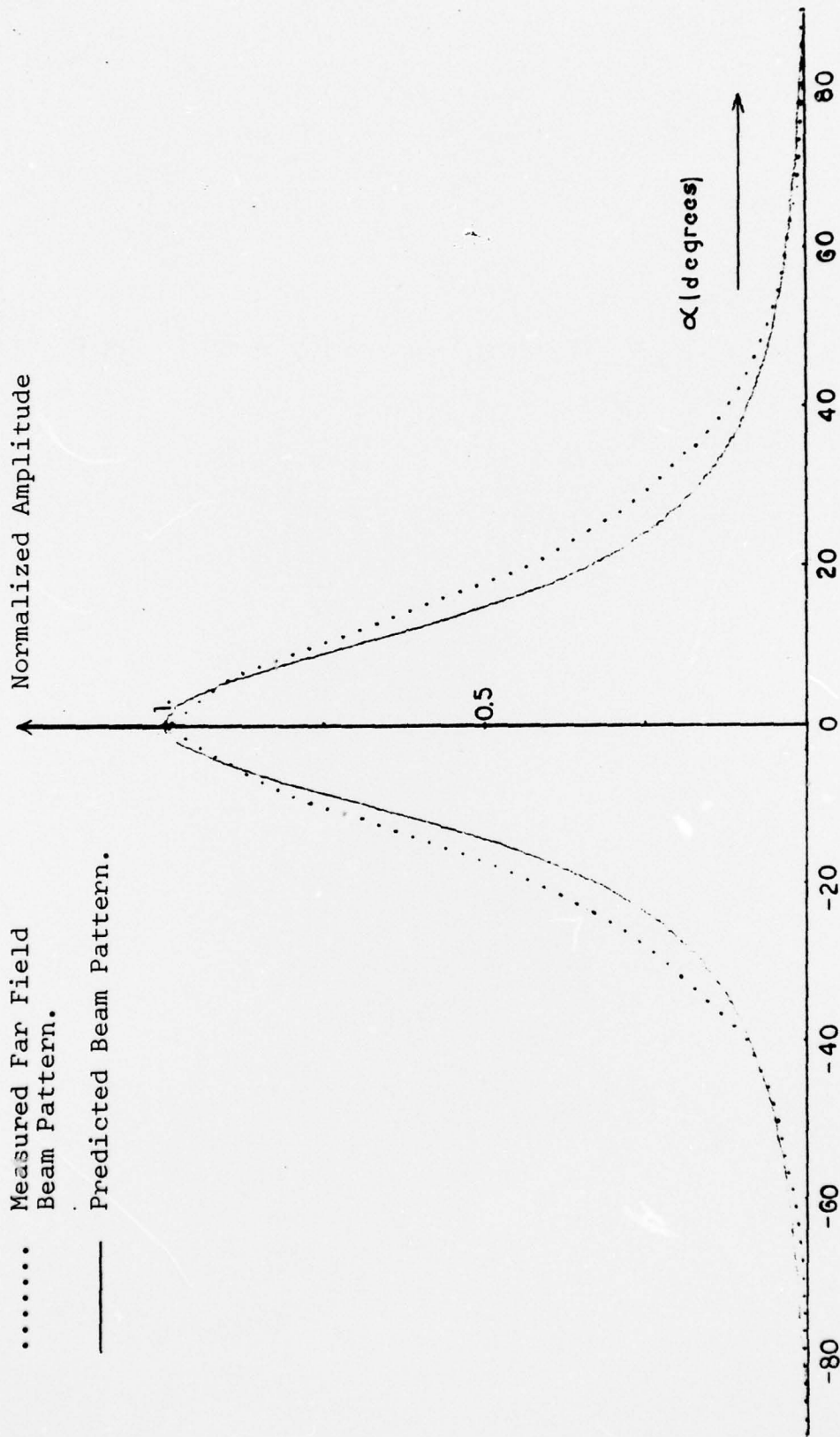


Figure 3.9 Predicted and measured beam pattern
 (UL = 4250 Hz, d = 12 cm, LL = 1100 Hz).

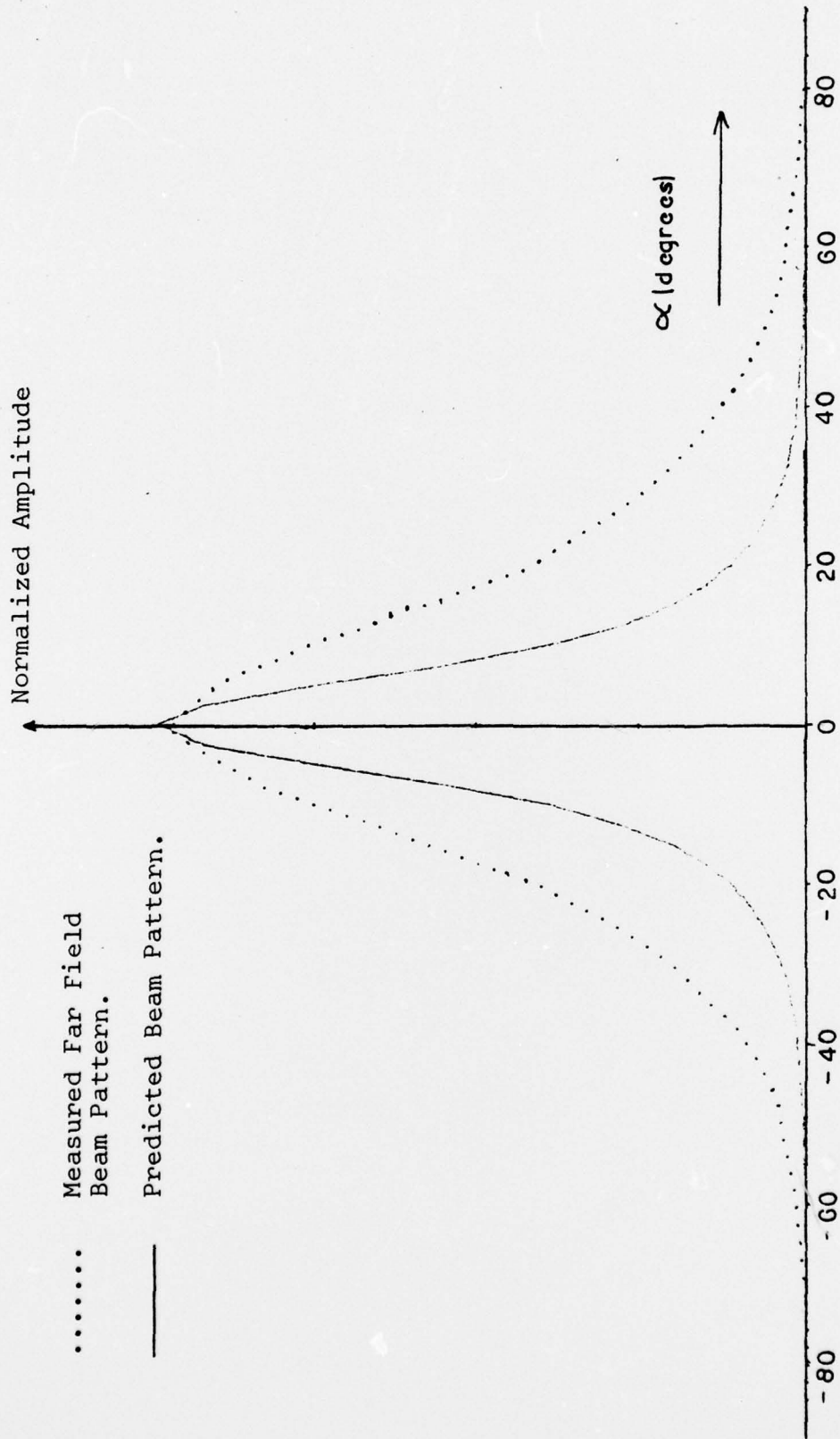


Figure 3.10 Predicted and measured beam pattern
 (UL = 4250 Hz, d = 15 cm, LL = 1100 Hz).

this parameter affects greatly the predicted width of the beam. This Figure also shows that the beam pattern is more sensitive to the correlation distance than to the limits of integration.

IV. CONCLUSION

The possibility of predicting the far field beam pattern from randomly vibrating surfaces has been demonstrated. It is feasible to obtain the intensity field and the radiation pattern from near field measurements of distributed sources. Although the theoretical model developed in Section II was tested experimentally with satisfactory results, more work needs to be done in both areas. The amount by which the beam pattern depends on each parameter makes it difficult to state a solid argument for describing the range of validity of each one.

The computed beam pattern was obtained solving equation (2.26) using a computer program for solving the integral by numerical methods. The limits of integration were chosen by means of the Frequency Spectrum, which was taken using a wave analyzer with automatic frequency sweep. The maximum range considered was from 1100 Hz to 5000 Hz. It was assumed that the frequencies producing the field were inside of this frequency band.

The mean square of the particle velocity, which has energy information, was shown to be related to the autocorrelation function. A correlator was used for that measurement and the power contained in the signal was easily calculated with equation (3.1). Note that in this case a correlator was

used but a true RMS voltmeter can also be used to measure the power of the signal.

The correlation distance was also measured with the correlator, a pair of microphones were located in the active area and the two dimensional (spatial and time) correlation function was observed. A correlation distance of 12 cm was used for calculation, but the measured value was found to vary with location of the microphones. The calculated beam pattern is very sensitive to this parameter. Its effects are bigger than those due to the limits of integration.

Different configuration of sources should be tested experimentally. Sources should be excited for different frequency bands in such a way as to produce an active region with a well defined correlation distance. This will solve one of the main problems of this experiment. Also it is suggested that the frequency spectrum of the configuration should not necessarily be continuous, as in this form the arrangement will be closer to real cases.

The theoretical model does not consider the spectrum level of the signal for the different frequencies. This should be tested more carefully in order to state a rule for the limits of integration. In the case of discontinuities in the Frequency Spectrum the model fails to give a straightforward solution, although it looks reasonable to perform a summation of the contribution of each frequency band. It was not possible to verify this concept with the experimental setup.

Agreement was generally good between measured and computed patterns, especially when the upper limit of integration was reduced to 4250 Hz. The actual beam pattern was slightly broader than the computed pattern in all cases. This is not surprising since the far field beam pattern depends on the frequency response of the source and the limits of integration were chosen in a rather empirical way, so the computed beam pattern could include a bigger frequency band than the real one and the width of the beam would be too narrow.

The technique developed here might also be useful in measuring the radiated noise pattern of submarines. Some additional considerations should be taken into account, and the theoretical model should be validated by actual measurement in anechoic tanks.


```

      BETA(74-I) = -BETA(I)
      P(74-I) = P(I)
      WRITE(6,100) Y,IER,BETA(I),P(I)
10  CONTINUE
100 FORMAT(/'Y =',E16.7,5X,'IER=',I5,5X,'BETA=',F7.2,'INT=
1  ',E16.7)

```

C
C
C
C
C
C

CALCULATE THE NORMALIZED AMPLITUDE OF THE PRESSURE FAR
FIELD BEAM PATTERN.

```

      Z = F(37)
      DO 20 I=1,73
      P(I) = ((P(I)/Z)**0.5)
      WRITE(6,200) BETA(I),P(I)
      P(I) = P(I)* 2.
20  CONTINUE
200 FORMAT(/,'BETA =',F7.2,13X,'NORMALIZED AMPLITUDE =',F
17.5)
      READ(5,50) TITLE
50  FORMAT(6A8)
      CALL DRAW(73,BETA,P,0,0,LABEL,TITLE,20.,0.5,0,4,0,2,
19,8,0,LAST)
      WRITE(6,400) LAST
400 FORMAT(/'LAST =',I2)
      STOP
      END

```

```

FUNCTION F(W)
IMPLICIT REAL*8 (A-P,O-Z)
COMMON D,C,RBETA,SN,PI
BIP = 0.5
BFP = 4250.
ERP = 2.
WP = BFP * PI * BRP
F = (W**2)/(((DEXP(BIP*((W*D/C)**2)*SN)))*(DEXP(BIP*
1((W/WP)**2))))
RETURN
END

```

LIST OF REFERENCES

1. C. W. Horton and G. S. Innis, Jr., "The Computation of Far-Field Radiation Patterns from Measurements Made Near the Source," The Journal of the Acoustical Society of America, v. 33, p. 877-880, July 1961.
2. D. D. Baker, "Determination of Far-Field Characteristics of Large Underwater Sound Transducers from Near-Field Measurements," The Journal of the Acoustical Society of America, v. 34, p. 1737-1744, November 1962.
3. R. J. Bobber, Underwater Electroacoustic Measurement, U. S. Government Printing Office, 1970.
4. F. R. Crawford, Submarine Radiated Noise Far-Field Beam Patterns for Discrete Frequencies from Near-Field Measurements, Thesis Naval Postgraduate School, December 1975.
5. H. W. Marsh, "Correlation in Wave Fields," USL Quarterly Report, Oct - Dec 1949, U. S. Navy Underwater Sound Laboratory.
6. G. B. Parrent, Jr., Journal of the Optical Society of America, 1959.
7. P. M. Morse and K. U. Ingard, Theoretical Acoustics, McGraw-Hill, 1968.
8. B. F. Cron and C. H. Sherman, "Spatial Correlation Function for Various Noise Models," The Journal of the Acoustical Society of America, v. 34, 1732-1736, November 1962.